

A surface chemical analysis strategy for the microstructural changes in a CuAgZrCr alloy cast under oxidation conditions

Ernesto G. Maffia^{1b}, Mercedes Muñoz^{2a}, Pablo A. Fetsis^{2c}, Carmen I. Cabello^{2,3a},
Delia Gazzoli^{4b} and Aldo A. Rubert^{*5}

¹Departamento de Mecánica de la Facultad de Ingeniería, Universidad Nacional de La Plata,
Calle 1 y 47 (1900)- La Plata, Buenos Aires, Argentina

²CINDECA-CCT- CONICET-CIC- Universidad Nacional de La Plata, Calle 47 N° 257 (1900)- La Plata,
Buenos Aires, Argentina

³Comisión de Investigaciones Científicas Pcia. Bs.As. CIC PBA Facultad de Ingeniería Universidad Nacional
de La Plata, Calle 1 y 47 (1900)- La Plata, Buenos Aires, Argentina

⁴Dipartimento di Chimica, "Sapienza" Università di Roma, Ple. Aldo Moro 5 (00185) Rome, Italy

⁵Instituto de Investigaciones Fisicoquímicas Teóricas y Aplicadas (INIFTA), Calle 64(SN) e/ Bv. 113 y 120,
Universidad Nacional de La Plata CONICET, (1900) La Plata, Buenos Aires, Argentina

(Received Decembet 12, 2022, Revised December 22, 2023, Accepted January 12, 2024)

Abstract. The aim of this work was to determine the behavior of alloy elements and compounds formed during solidification in the manufacturing process of the CuAgZrCr alloy under an oxidizing environment. Bulk and surface analysis techniques, such as Scanning Electron Microscopy (SEM), X-ray Photoelectron Spectroscopy (XPS), Raman and X-ray diffraction (XRD) were used to characterize the phases obtained in the solidification process. In order to focus the analysis on the on grain boundary interface, partial removal of the matrix phase by acid attack was performed. The compositional differences obtained by SEM-EDX, Raman and XPS on post-manufacturing materials allowed us to conclude that the composition of grain boundaries of the alloy is directly influenced by the oxidizing environment of alloy manufacturing.

Keywords: intermetallic phases; microstructure CuAgZrCr cast-alloy; surface chemical analyses

1. Introduction

Cu-Ag alloys are among some of the most promising materials used as electric conductors, mainly because tensile strength of 1GPa and 60% IACS (International Annealed Copper Standard) can be achieved (Lin and Meng 2008). When these alloys are manufactured with the addition of elements such as Zr and Cr, a temperature resistant material is obtained, which is also useful for the aerospace industry. The result of the chemical interaction between the elements results in a class of compounds called intermetallics, some of their beneficial effects being the increase in mechanical

*Corresponding author, Professor, E-mail: rubert@quimica.unlp.edu.ar

^aPh.D.

^bProfessor

^cGraduate in Chemistry

properties. According to Krishna *et al.* (2013) it is possible to model the shape and size of intermetallics by heat treatment and approximately spherical shapes with diameters of 9.0 ± 2.0 nm can be achieved by applying heat treatments. However, particle precipitation through heat treatment is not the only way to increase properties. Cold working also produces the same result (Krishna *et al.* 2014). In the same sense, Wu *et al.* (2023), demonstrated that the application of multistage thermal mechanical treatments generates a substantial improvement in properties. The intermetallic particles have a coherent interphase when first formed during heat treatment (Haasen 1996). In the case of the CuAgZr alloy, good tensile strength, corrosion and oxidation resistance at high temperatures, high resistance to thermal fatigue working both at high or low cycle number, and most importantly, a high thermal and electrical conductivity are achieved. The CuAgZr alloy is hardened by heat treatment, yielding a material capable of withstanding high thermal loads, suitable for the manufacturing of molds for plastic packaging. The precipitates responsible for the hardening effect are, according to Jia *et al.* (2009) intermetallic species of Cu₅Zr composition, with fcc (face-centered cubic) structure and a coherent interphase. According to Tian *et al.* (2018) this phase manifests also in high CrCuCrZr alloy, where the Zr addition forms the CuZr phase. Intermetallics as well as Ag nanoparticles cause a strengthening mechanism in the CuAgZr alloy. The results from Wu *et al.* (2019) indicate that the Cu-3 wt% Ag-1 wt% Zr contains nanometric Ag precipitates uniformly distributed throughout the structure and also Cu₄AgZr particles of micrometric size. However, intermetallic compounds are not always beneficial for the properties of an alloy because in occasions they negatively affect corrosion resistance. (Ma *et al.* 2015) investigated the intermetallic particles behavior towards corrosion, finding that intermetallics produce shallow pitting. This, though being an inconvenience, can be turned into a benefit when the influence of thermomechanical treatments in the surface quality of the material is evaluated. Surface degradation of an Ag₂Sn₄La alloy exposed to highly oxidizing environments has been investigated by Zhao *et al.* (2018). These researchers observed that intermetallics suffer preferential oxidation, which is not a benefit for the material microstructure design. Improvement of electric conductivity besides an increase in mechanical resistance of a CuAg alloy properties by the joint addition of Cr and Zr was reported by Liu *et al.* (2012). These authors proved that not only Cu- and Zr-rich particles formed, but also altered the amount of Ag-rich phase in a Cu-6%Ag alloy, which is suggested as responsible for the property changes.

As for the CuAgZrCr alloy studied in this work, it is known that the first solid to nucleate is copper which will contain some oxide species due to the exposure to the atmosphere during the casting process (Abbaschian and Reed-Hill 2008). Larger scale preparation in an inert atmosphere is an expensive route. When the oxides formed are not reduced at the right time, new species of combinations are produced between the added elements and the existing oxides. Precipitates in grain boundaries will be the final results in the formation of composites. These precipitated phases may cause inconveniences during the forming process and heat treatment. Thus, this issue requires special attention to determine the microstructural evolution and property of the alloy.

In the present work, the characterization of a CuAgZrCr alloy, to determine the aforementioned behavior of its alloy elements in an oxidizing manufacturing environment was studied. The characterization by bulk and surface techniques including X-ray diffraction (XRD), Scanning Electron Microscopy (SEM), X-ray Photoelectron Spectroscopy (XPS) and Raman allowed us to identify the compounds formed in the process of fusion and solidification of the CuAgZrCr alloy.

2. Preparation procedures

The alloy studied was prepared in a copper load maximum 50 Kg inductive half frequency furnace operating to open atmosphere. Refined copper and commercially pure ingots of silver (99,99% R.Cordes.S.A.) chromium (99.45%) and zirconium (99.8%-from Indium Corp USA.) were used and the liquid copper deoxidation process was carried out with lithium (99,95%) and phosphorus (Cu-P master alloy Sichuan-Lande Industry, P content 14~16%). Melting process starts with copper ingot in a graphite crucible at 1200°C. Liquid copper formed was protected with carbon powder to prevent a massive loss of copper by oxidation. Silver was added through the graphite bell and then deoxidation was performed. Finally, zirconium and chromium ingots were added to the casting.

A thermal treatment was carried out at 900°C for 1 hour and subsequent rapid cooling with water. This procedure was carried out to improve the hardness by the precipitation method, the temperature was chosen based on the Cu-Ag phase diagram and the composition found (Perepezko and Subramanian 1992). Subsequently, two heating cycles at 450°C for 4.5 hours and quenching in water were used to maximize the resistance of the material obtained, named aged alloy. Some aged alloy samples were treated for 30 seconds with a drop of concentrated nitric acid (~65% Carlo Erba P.A.), washed with distilled water, and then dried. This treatment is referred to as etching. This etching is intended to dissolve copper, the major component of the alloy, and to expose the grain boundary in the microstructure for a more focused study of its phases and their composition.

3. Characterization methods

Chemical composition was determined through X-ray fluorescence (Bruker S Titan equipment). Samples were characterized by a Scanning Electron Microscopy with a SEM Philips 505 device equipped with a dispersive energy microanalysis system EDAX 9100. XRD patterns were obtained with a Philips PW 1729 diffractometer using Cu K α (Ni-filtered) radiation in the 5-60° 2 θ range (step size 0.02°; time per step 1.25 s). Because the alloy fragments were not completely flat, each sample was exposed to the X-rays adopting different orientations to check composition homogeneity. Mean crystallite diameter (d) was calculated by the Scherrer equation (Scherrer 1918) as $d = \lambda K / \beta \cos \theta$, where K is a shape constant equal to 0.9, λ the wavelength of the X-ray used, and $\beta \cos \theta$, where the effective linewidth (FWHM) of the observed X-ray reflection, obtained by curve-fitting procedure after Warren's correction for instrumental broadening and background subtraction.

Raman spectra were measured at room temperature in back-scattering geometry with an in Via Renishaw Micro-Raman spectrometer equipped with an air-cooled CCD detector and edge filters. The emission line at 488.0 nm from an argon ion laser was focused on the sample under a Leica DLML microscope using 20 \times or 5 \times objectives. The power of the incident beam was about 5 mW. Five 10 s accumulations were generally acquired for each sample. The resolution was 2 cm⁻¹ and spectra were calibrated using the 520.5 cm⁻¹ line of a silicon wafer. Spectra processing included baseline removal and curve fitting using a Gauss-Lorentz cross-product function by Peakfit 4.12 software (Systat Software Inc. 2007).

X-ray photoelectron Spectroscopy (XPS) measurements were carried out with dual nonmonochromatic Mg/Al K α source (XR50, Specs GmbH) and a hemispherical electron energy analyser (PHOIBOS 100, Specs GmbH) in fixed transmission analysis mode (FAT) operating at 40 and 20 eV pass energy. A two-point calibration of the energy scale was performed using sputtered cleaned gold (Au 4f_{7/2}, binding energy BE=84.00 eV) and copper (Cu 2p_{3/2}, BE=932.67 eV) samples. The take-off angle for analysis was 90° and adventitious carbon (component C1s at 284.8 eV) was

Table 1 Composition of aged alloy in wt%, determined by X-ray fluorescence

Alloying elements	Chromium	Copper	Phosphorus	Silver	Zirconium
Composition (wt%)	0.255	rest	0.395	2.86	0.75

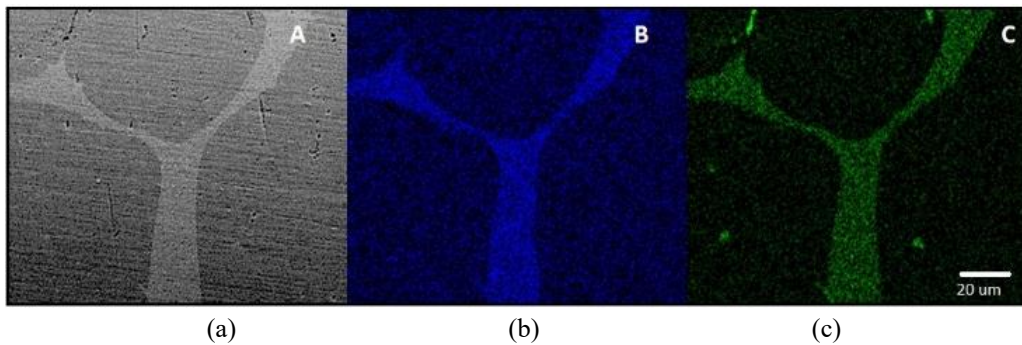


Fig. 1 (a) Panel A: EDS micrograph of the aged CuAgZrCr alloy, (b) Panel B: The blue region shows the content of Ag as continuous phase at the grain boundary and (c) Panel C: The green one indicates the Zr region.

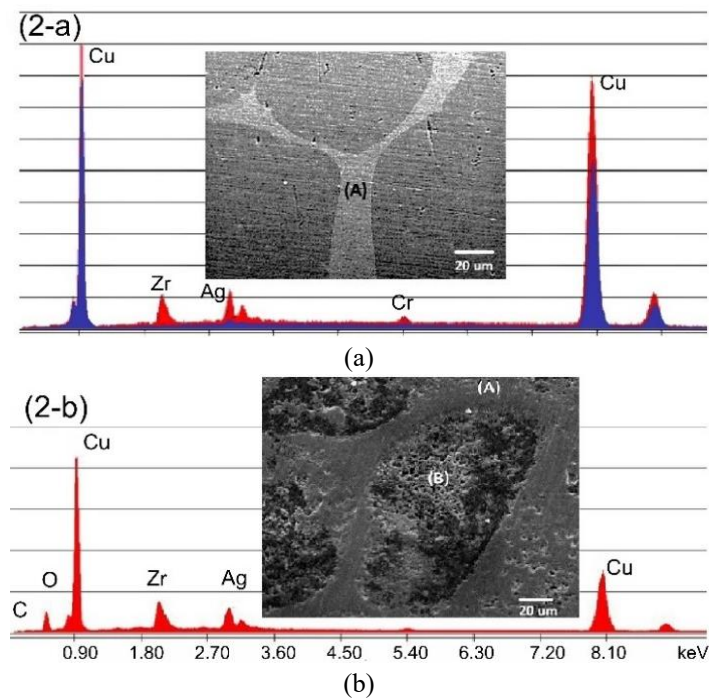


Fig. 2 (a) SEM-EDS element composition of a grain (light blue) and grain boundary (red) of the CuAgZrCr alloy (The selected grain boundary zone in the micrograph is referenced with the letter A.) and (b) Idem with etched alloy on zone A

used as charging reference when required. The pressure was typically in the 10^{-9} mbar range for all measurements. XP spectra were analysed with CASA-xps v2.2.99 software. The quantification analysis by peak areas and relative sensitivity factor was employed.

4. Results

The chemical composition achieved in the casting procedure of the CuAgZrCr aged alloy is reported in Table 1.

4.1 SEM-EDS micrographics analysis

4.1.1 Aged alloy

The SEM-EDS micrograph of the aged alloy, clearly shows that there is a continuous phase at grain boundaries, Fig. 1. The treatment at 900°C does not dissolve this phase since it appears in a continuous mode at the grain boundaries. The EDS mapping shows the distribution of the Ag and Zr in the structure of the alloy, Fig. 1 (panel B and C, respectively).

No Cr is found on mapping the aged sample. Fig. 2(a) shows no P on these regions, although P may be masked by Zr at the grain boundaries.

4.1.2 Etched alloy

Fig. 2(b) shows a SEM micrograph of the etched CuAgZrCr alloy. In order to restrict the analysis to the grain boundary phase, the remaining phase was partially removed by nitric acid attack. The topography clearly shows two distinct zones: a continuous grain boundary (“A” label) and a porous zone (“B” label) corresponding to the grain etching. This allows for clear determination of size and shape of alloy grains (grain diameter is above 50 μm). EDS analysis of zone “A” shown in Fig. 2(b), confirms the presence of elements such as Cu, Ag, Zr, O.

4.2 XRD analysis

A representative X-Ray diffraction pattern of the aged alloy is illustrated in Fig. 3(a). Besides the reflections at 2θ values of 43.3° and 50.4° assigned to the (111) and (200) crystallographic planes of Cu (JCPDF cards 4-0836), sharp and low intensity peaks at 2θ values of 38.1° and 44.6° ascribed to the (111) and (200) planes of Ag (JCPDF cards 4-0783) were detected. The average crystallite size of Ag, determined by the Scherrer equation using the (111) reflection, resulted to be 110 nm. The XRD diffraction pattern of the alloy etched with nitric acid is shown in Fig. 3(b). No reflections other than those at 2θ values of 43.3° and 50.4° assigned to the (111) and (200) crystallographic planes of Cu (JCPDF cards 4-0836) are detected. However, as shown in the inset of Fig. 3(b), a closer inspection of the pattern in the 2θ range 24° - 34° disclosed very weak and broad features at 2θ 28.2° and 31.5° assigned to the most intense reflection of ZrO_2 in the monoclinic crystallographic phase (JCPDF cards 36-420).

4.3 Raman analysis

4.3.1 Aged alloy

Raman scattering, applied to identify oxide-based components of the aged CuAgZrCr alloy surface, revealed main bands at about 147, 218, 418, 525, 635 cm^{-1} and broad low intensity features in the 800-1200 cm^{-1} range, Fig. 4. The main bands can be attributed to Cu-O and Ag-O vibrations modes whereas the low intensity ones to molecular species on the alloy surface (molecular oxygen, phosphates, and carbonates). To better identify the various components arising from the relevant

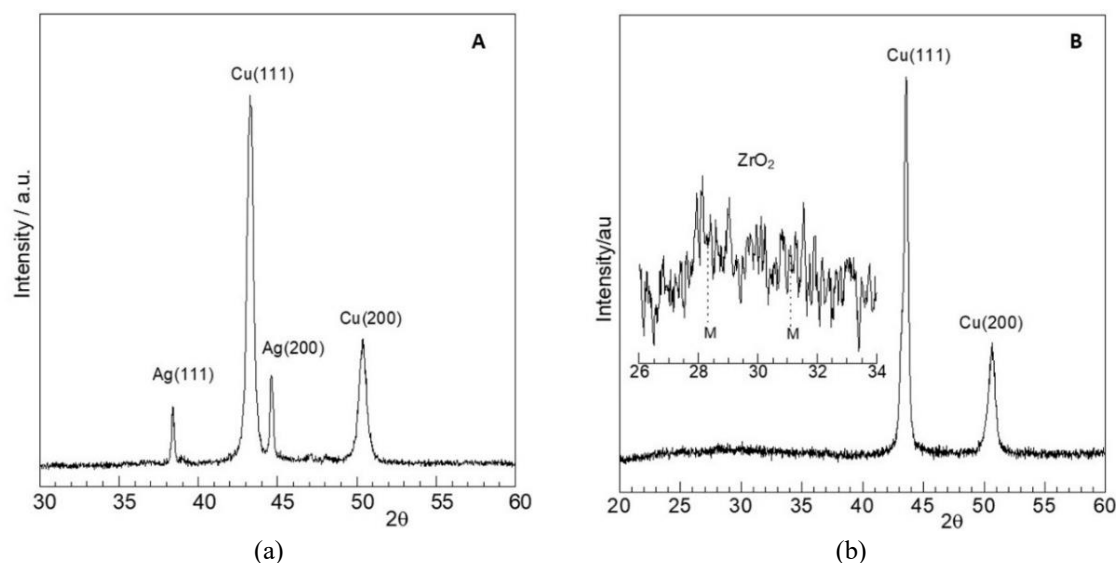


Fig. 3 (a) XRD pattern of the aged CuAgZrCr alloy and (b) XRD pattern of CuAgZrCr alloy after etching (Inset highlights ZrO_2 monoclinic modification.)

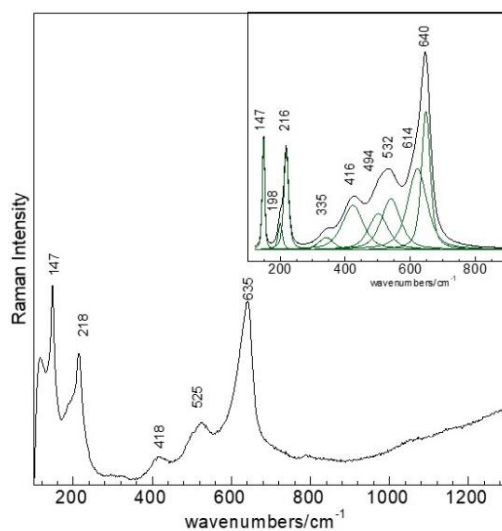


Fig. 4 A representative Raman spectrum of the CuAgZrCr aged alloy (Inset: curve fitting of the $100\text{-}900\text{ cm}^{-1}$ region after background subtraction.)

elements a curve fitting procedure was applied to the spectrum in the $100\text{-}900\text{ cm}^{-1}$ range, Fig. 4 (inset).

According to the literature, Raman analysis disclosed the presence of Ag_2O [$147, 494\text{ cm}^{-1}$ (Martina *et al.* 2012, Waterhouse *et al.* 2003, 2001)], AgO [$(216, 416\text{ cm}^{-1})$; (Waterhouse *et al.* 2003, Ravi Chandra *et al.* 2009)], Cu_2O [$216, 532, 614\text{ cm}^{-1}$ (Xu *et al.* 1999)] and ZrO_2 in the monoclinic modification [$198, 335, 616$ and 640 cm^{-1} ; (Gazzoli *et al.* 2007)]. No evidence of CuO is obtained as the most intense band at 298 cm^{-1} is missing (Xu *et al.* 1999, Karle *et al.* 2017).

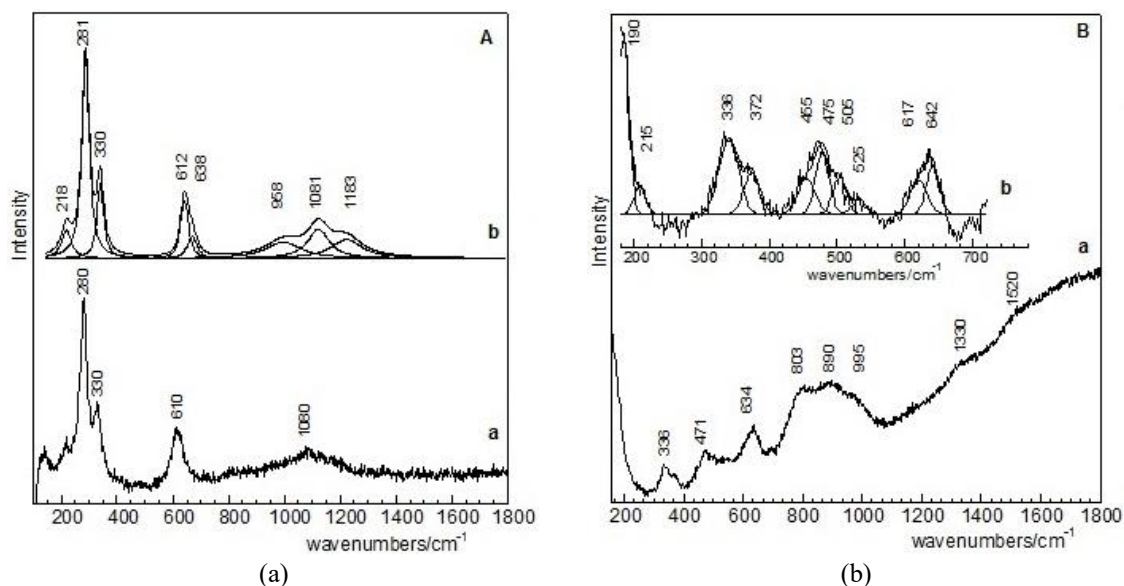


Fig. 5 Representative Raman spectrum of groups (a) A and (b) B Raman on CuAgZrCr alloy after HNO₃ etching (Curve a: Rough spectrum, Curve b: Curve fitting components after background subtraction)

4.3.2 Etched alloy

Raman spectra of the alloy after treatment with nitric acid varied in composition and background intensity, depending on the analyzed area (5 \times and 20 \times objectives). These findings suggest a heterogeneous sample surface, in agreement with SEM micrographs. Spectra were split in two groups referred to as A and B, same to Fig. 2, one characterized by sharp bands and smooth background (group A) while the other one by broad and low intensity bands superimposed to high intensity background (group B).

In Fig. 5(a), a typical Raman spectrum of group A is shown, exhibiting sharp peaks at about 280, 330, 610 cm⁻¹ and a broad composite band centered at about 1080 cm⁻¹ (curve a). Peak fitting analysis (curve b) yielded components assigned to CuO (281, 330 and 605 cm⁻¹; Xu *et al.* 1999) and to Cu₂O [218 and 620 cm⁻¹ (Xu *et al.* 1999, Karle *et al.* 2017)]. The broad and low intensity bands at 958, 1081 and 1183 cm⁻¹ have been proposed to arise from adsorbed carbonate species and oxygen species adsorbed at the grain boundary of silver (Waterhouse *et al.* 2003).

A representative Raman spectrum of group B (Fig. 5(b), curve a) shows sharp peaks at about 336, 471, 634 cm⁻¹, a broad composite band (803, 890, 995 cm⁻¹) and a steep background. Peak fitting analysis (Fig. 5(b), curve b) disclosed the presence of components originating from AgO [216, 372, 455, 502 cm⁻¹; (Waterhouse *et al.* 2003, Ravi Chandra *et al.* 2009)], Cu₂O [215, 531, 617, 638 cm⁻¹ (Xu *et al.* 1999)] and to ZrO₂ monoclinic modification [190 339 372, 475, 617, 638 cm⁻¹ (Gazzoli *et al.* 2007)]. In addition, the broad and low intensity bands at 803, 890 and 995 cm⁻¹ arise from oxygen species adsorbed at the metal silver grain boundary or an incipient silver oxidation zone (Waterhouse *et al.* 2003).

Comparing the results obtained before and after etching, it can be concluded that the etching treatment causes surface heterogeneity and appearance of CuO species.

4.4 XPS analysis

Table 2 Relative atomic composition (At%) of CuAgZrCr alloys by XPS.

Elements	Ag	C	Cr	Cu	O	P	Zr	N
Aged	0.2	54.9	-	15.3	29.4	-	0.1	-
Etched	-	38.4	-	7.8	46.5	-	1.9	5.4

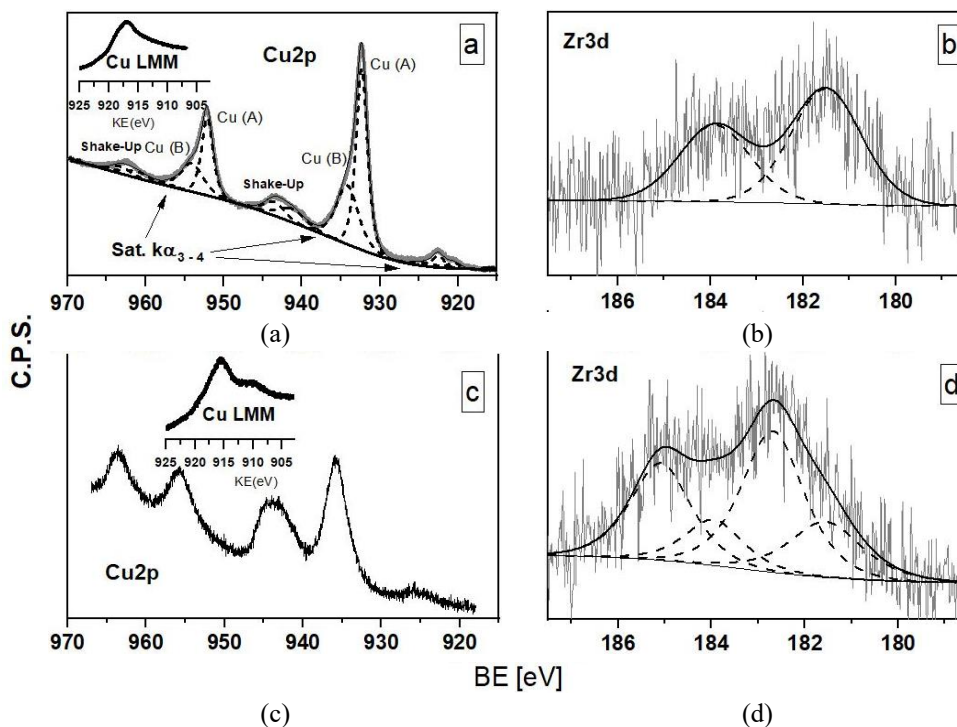


Fig. 6 (a) and (b) Fitting components of the Cu₂p and Zr 3d XPS regions for Cu-Ag-Zr aged alloy, (c) and (d) Etched alloy (Insets: Auger signal Cu LMM on kinetic energy (KE) representation, BE: Binding energy, C.P.S.: Counts per seconds)

XPS is a surface-sensitive technique, probing the outermost 5-10 nm of the alloy (Briggs and Seah 1990). In this work, it has been used to determine the effect of etching on the alloy surface. Table 2 shows the relative values of atomic composition. An increase in the Zr signal after etching is shown. The disappearance of the Ag signal and the decrease of the Cu signal are also notable.

4.4.1 Aged alloy

Analysis of the Cu₂p signal is shown in Fig. 6(a). Data fit was attained with two main peaks named A and B with binding energies for the component 2p_{3/2} of 932.32 and 934.17 eV respectively. A Shirley background line was used.

The 2p_{3/2}-2p_{1/2} doublet separation values were found in 19.9 eV. Peak B was assigned to Cu(II) and the shake-up satellites were fitted with two peaks. Since Cu(I) and Cu(0) are indistinguishable from the photoelectronic signal (Tobin *et al.* 1983) the Auger parameter for Cu in this alloy was determined, resulting with a value of 1849.32 eV very close to that expected for Cu(I) species, as

reported by Tobin *et al.* (1983). Fig. 6(b) shows data and fitting for the Zr 3d signal. A doublet, with a 2.4 eV spin orbit splitting was needed for fitting. The maximum for the 3d_{5/2} signal is found at a binding energy of 181.5 eV. Morant *et al.* (1989) identified this signal for the Zr(II) species.

4.4.2 Etched alloy

Fig. 6(c) shows rough data for the Cu-2p region. The binding energy of the Cu 2p_{3/2} region was found at 935.82 eV, and the typical shake-up peak due to Cu(II) was present. The Auger parameter for Cu is 1851.06 eV, close to that of CuO as reported by (Tobin *et al.* 1983, Van Ooij 1977).

Therefore, the surface of the alloy etched with HNO₃ shows Cu(II) mostly. The etched alloy still has some copper after brief acid attack as shown in Table 2. The Zr spectra of the etched alloy shows a new species with a higher oxidation state than the aged alloy (see Fig. 6(d)). The main doublet corresponds to a formal state between Zr(III) and Zr(IV) as reported by (Azdad *et al.* 2018, Morant *et al.* 1989). This state can be attributed to non-stoichiometric oxides of the most superficial exposed layers.

5. Conclusions

In this work, a CuAgCrZr alloy, manufactured under oxidation conditions in an induction furnace at a preparative scale, with the deoxidation process and thermal post-treatment, has been characterized. Strategies to economize the synthesis in an open atmosphere, on a preparative scale, consisted of the deoxidation of Cu with Li and P and cast protection with carbon powder. The methods used to characterize the materials did not show impurities other than those of the materials used in the foundry (crucible, tools, flux, etc.) except oxygen in the quantities reported. We found that the microstructure and composition of the surface aged alloy has more Ag and Zr at the grain boundary than in the grain body.

The aged alloy appears to be composed of a solid solution of copper with Ag dispersed throughout the surface bulk structure with the largest amount at the grain boundary, as reported by Jia *et al.* (2009) for similar alloys that achieve maximum strength by thermal posttreatment. XRD shows the presence of silver dispersed on aged alloy with an average size of around 110 nm, which supports this idea.

Raman analysis of the aged alloy revealed the presence of molecular species involving Cu-O, Ag-O vibrations modes (Ag₂O, AgO, Cu₂O) and Zr-O modes typical of the monoclinic modification. ZrO₂ in the monoclinic modification was also barely detected by XRD. For the etched alloy, in agreement with SEM-EDS investigation, an extensive surface heterogeneity was apparent, containing different oxidized species (AgO, Cu₂O, CuO and ZrO₂) in addition to adsorbed carbonate species and oxygen species adsorbed at the silver grain boundaries.

XPS shows that the aged alloy presents a typical surface layer of CuO mainly. Zirconium was found as Zr(II), while higher oxidation states were found in the etched alloy. The amount of silver at the analyzed interface by XPS was too low to determine its oxidation state and no Cr was detected at this interface. The copper in the etched alloy is entirely Cu(II), and etching removed all traces of Ag. Etching eliminates most grains of the CuAgZrCr alloy and depletes the Ag, but not the Zr, and therefore the grain boundary contains the Zr compounds after etching. We attribute the chemical resistance of the grain boundary to the Zr components present. This agrees with the EDS characterization indicating a higher concentration of Zr at the grain boundary of the aged alloy. We found evidence of Cr by EDS at the grain boundary. Zirconium preferentially reacts with oxygen

during the melting process, but oxygen still remains. We attribute this excess oxygen to the difficulty of transferring the protected molten alloy to a mold in an open atmosphere.

We conclude that the effect of thermal post-treatment on Ag dissolution could be studied in this type of alloy because the characterization techniques used combined with the nitric etching strategy were useful to understand the generation of CuAgZrCr compounds, such as the oxidized species that remain within the grain boundaries and alter the final properties of the alloy.

Acknowledgments

The authors wish to thank to Universidad Nacional de La Plata (UNLP) of Argentina I207 Project for the financial support provided for the realization of this research work. The authors wish to thank the research unit PROINTEC I&D of Facultad de Ingeniería of La Plata, UNLP for facilitating the use of their equipment and the material used in this work. The authors thank Consejo Nacional de Investigaciones Científicas y Técnicas (CONICET).

References

- Abbaschian, R. and Reed-Hill, R.E. (2008), *Physical Metallurgy Principles*, Course Technology, Boston, MA, USA.
- Azdad, Z., Marot, L., Moser, L., Steiner, R. and Meyer, E. (2018), “Valence band behaviour of zirconium oxide, Photoelectron and Auger spectroscopy study”, *Sci. Rep.*, **8**(1), 16251. <https://doi.org/10.1038/s41598-018-34570-w>.
- Briggs, D. and Seah, M.P. (1990), *Practical Surface Analysis Volume 1 -Auger and X-Ray Photoelectron Spectroscopy*, 2nd Edition, John Wiley & Sons Ltd, Chichester, UK.
- Gazzoli, D., Mattei, G. and Valigi, M. (2007), “Raman and X-ray investigations of the incorporation of Ca²⁺ and Cd²⁺ in the ZrO₂ structure”, *J. Raman Spectrosc.*, **38**, 824-831. <https://doi.org/10.1002/JRS.1708>.
- Haasen, P. (1996), “Mechanical properties of solid solutions”, *Physical Metallurgy*, 4th Edition, Elsevier, Amsterdam, Netherlands.
- Jia, S.G., Ning, X.M., Liu, P., Zheng, M.S. and Zhou, G.S. (2009), “Age hardening characteristics of Cu-Ag-Zr alloy”, *Met. Mater. Int.*, **15**, 555-558. <https://doi.org/10.1007/s12540-009-0555-0>.
- Karle, S., Rogalla, D., Ludwig, A., Becker, H.W., Wieck, A.D., Grafen, M., Ostendorf, A. and Devi, A. (2017), “Synthesis and evaluation of new copper ketoiminate precursors for a facile and additive-free solution-based approach to nanoscale copper oxide thin films”, *Dalt. Trans.*, **46**(8), 2670-2679. <https://doi.org/10.1039/C6DT04399B>.
- Krishna, S.C., Gangwar, N.K., Jha, A.K., Pant, B. and George, K.M. (2014), “Properties and strengthening mechanisms in cold rolled and aged Cu-3Ag-0.5Zr alloy”, *Metallogr. Microstruct. Anal.*, **34**(3), 323-327. <https://doi.org/10.1007/S13632-014-0147-3>.
- Krishna, S.C., Tharian, K.T., Pant, B. and Kottada, R.S. (2013), “Microstructure and mechanical properties of Cu-Ag-Zr alloy”, *J. Mater. Eng. Perform.*, **22**, 3884-3889. <https://doi.org/10.1007/s11665-013-0659-z>.
- Lin, J. and Meng, L. (2008), “Effect of aging treatment on microstructure and mechanical properties of Cu-Ag alloys”, *J. Alloys Compd.*, **454**, 150-155. <https://doi.org/10.1016/J.JALLCOM.2006.12.073>.
- Liu, J.B., Zhang, L., Dong, A.P., Wang, L.T., Zeng, Y.W. and Meng, L. (2012), “Effects of Cr and Zr additions on the microstructure and properties of Cu-6 wt.% Ag alloys”, *Mater. Sci. Eng. A*, **532**, 331-338. <https://doi.org/10.1016/J.MSEA.2011.10.099>.
- Ma, Y., Zhou, X., Huang, W., Thompson, G.E., Zhang, X., Luo, C. and Sun, Z. (2015), “Localized corrosion in AA2099-T83 aluminum-lithium alloy: The role of intermetallic particles”, *Mater. Chem. Phys.*, **161**, 201-210. <https://doi.org/10.1016/J.MATCHEMPHYS.2015.05.037>.

- Martina, I., Wiesinger, R., Jembrih-Simbuenger, D. and Schreiner, M. (2012), "Micro-Raman characterisation of silver corrosion products", *E Preserv. Sci.*, **9**, 1-8.
- Morant, C., Sanz, J.M., Galán, L., Soriano, L. and Rueda, F. (1989), "An XPS study of the interaction of oxygen with zirconium", *Surf. Sci.*, **218**, 331-345. [https://doi.org/10.1016/0039-6028\(89\)90156-8](https://doi.org/10.1016/0039-6028(89)90156-8).
- Perepezko, P.R. and Subramanian, J.H. (1992), *ASM Handbook Volume 3: Alloy Phase Diagrams*, ASM International, Materials Park, OH, USA.
- Ravi Chandra Raju, N., Jagadeesh Kumar, K. and Subrahmanyam, A. (2009), "Physical properties of silver oxide thin films by pulsed laser deposition: Effect of oxygen pressure during growth", *J. Phys. D: Appl. Phys.*, **42**(13), 135411. <https://doi.org/10.1088/0022-3727/42/13/135411>.
- Scherrer, P. (1918), "Bestimmung der Grosse und der Inneren Struktur von Kolloidteilchen Mittels Rontgenstrahlen", *Nach Ges Wiss Gottingen*, **2**, 8-100.
- Tian, W., Bi, L., Ma, F. and Du, J. (2018), "Effect of Zr on as-cast microstructure and properties of Cu-Cr alloy", *Vacuum*, **149**, 238-247. <https://doi.org/10.1016/J.VACUUM.2017.12.011>.
- Tobin, J.P., Hirschwald, W.H. and Cunningham, J. (1983), "XPS and XAES studies of transient enhancement of CuI at CuO surfaces during vacuum outgassing", *Appl. Surf. Sci.*, **16**, 441-452. [https://doi.org/10.1016/0378-5963\(83\)90085-5](https://doi.org/10.1016/0378-5963(83)90085-5).
- Van Ooij, W.J. (1977), "Surface composition, oxidation and sulfidation of cold-worked brass and brass-coated steel wire as studied by x-ray photoelectron spectroscopy I. Surface composition of commercial cold-worked brass", *Surf. Technol.*, **6**, 1-18. [https://doi.org/10.1016/0376-4583\(77\)90019-X](https://doi.org/10.1016/0376-4583(77)90019-X).
- Waterhouse, G.I.N., Bowmaker, G.A. and Metson, J.B. (2001), "The thermal decomposition of silver (I, III) oxide: A combined XRD, FT-IR and Raman spectroscopic study", *Phys. Chem. Chem. Phys.*, **3**, 3838-3845. <https://doi.org/10.1039/B103226G>.
- Waterhouse, G.I.N., Bowmaker, G.A. and Metson, J.B. (2003), "Oxygen chemisorption on an electrolytic silver catalyst: a combined TPD and Raman spectroscopic study", *Appl. Surf. Sci.*, **214**, 36-51. [https://doi.org/10.1016/S0169-4332\(03\)00350-7](https://doi.org/10.1016/S0169-4332(03)00350-7).
- Wu, X., Wang, R., Peng, C., Feng, Y. and Cai, Z. (2019), "Effects of annealing on microstructure and mechanical properties of rapidly solidified Cu-3 wt% Ag-1 wt% Zr", *Mater. Sci. Eng. A*, **739**, 357-366. <https://doi.org/10.1016/J.MSEA.2018.10.062>.
- Wu, Z., Hu, J., Xin, Z., Qin, L., Jia, Y. and Jiang, Y. (2023), "Microstructure and properties of Cu-Zn-Cr-Zr alloy treated by multistage thermo-mechanical treatment", *Mater. Sci. Eng. A*, **870**, 144679. <https://doi.org/10.1016/j.msea.2023.144679>.
- Xu, J.F., Ji, W., Shen, Z.X., Li, W.S., Tang, S.H., Ye, X.R., Jia, D.Z. and Xin, X.Q. (1999), "Raman spectra of CuO nanocrystals", *J. Raman Spectrosc.*, **30**(5), 413-415. [https://doi.org/10.1002/\(SICI\)1097-4555\(199905\)30:5<413::AID-JRS387>3.0.CO;2-N](https://doi.org/10.1002/(SICI)1097-4555(199905)30:5<413::AID-JRS387>3.0.CO;2-N).
- Zhao, Q., Liu, H., Wu, C., Li, N., Jiang, Y. and Yi, D. (2018), "Preferential oxidation of intermetallic compounds in Ag-2Sn-4La alloy", *Corros. Sci.*, **143**, 177-186. <https://doi.org/10.1016/J.CORSCI.2018.08.017>.